

Structural and electrical characteristics of rapid thermally processed ferroelectric Bi₄Ti₃O₁₂ thin films prepared by metalorganic solution deposition technique

P. C. Joshi and S. B. Desu

Citation: [Journal of Applied Physics](#) **80**, 2349 (1996); doi: 10.1063/1.363069

View online: <http://dx.doi.org/10.1063/1.363069>

View Table of Contents: <http://scitation.aip.org/content/aip/journal/jap/80/4?ver=pdfcov>

Published by the [AIP Publishing](#)

Articles you may be interested in

[Effect of CeO₂ interlayer deposition temperature on growth behavior of Bi₄Ti₃O₁₂/CeO₂/MgO heterostructures](#)
Appl. Phys. Lett. **69**, 1077 (1996); 10.1063/1.117063

[Electrical properties of \(Zr,Sn\)TiO₄ dielectric thin film prepared by pulsed laser deposition](#)
J. Appl. Phys. **80**, 388 (1996); 10.1063/1.362795

[Structural and optical properties of laser deposited ferroelectric \(Sr_{0.2}Ba_{0.8}\)TiO₃ thin films](#)
J. Appl. Phys. **79**, 7965 (1996); 10.1063/1.362346

[Structural and dielectric studies of Pb\(Mg_{1/3}Nb_{2/3}\)O₃-PbTiO₃ ferroelectric solid solutions around the morphotropic boundary](#)
J. Appl. Phys. **79**, 4291 (1996); 10.1063/1.361865

[Postgrowth annealing effects of TiO₂ thin films grown on InP substrate at low-temperature by metal-organic chemical-vapor deposition](#)
J. Appl. Phys. **79**, 4459 (1996); 10.1063/1.361757

MIT LINCOLN
LABORATORY
CAREERS

Discover the satisfaction of
innovation and service
to the nation

- Space Control
- Air & Missile Defense
- Communications Systems & Cyber Security
- Intelligence, Surveillance and Reconnaissance Systems
- Advanced Electronics
- Tactical Systems
- Homeland Protection
- Air Traffic Control

 **LINCOLN LABORATORY**
MASSACHUSETTS INSTITUTE OF TECHNOLOGY



Structural and electrical characteristics of rapid thermally processed ferroelectric $\text{Bi}_4\text{Ti}_3\text{O}_{12}$ thin films prepared by metalorganic solution deposition technique

P. C. Joshi^{a)} and S. B. Desu

Department of Materials Science and Engineering, Virginia Polytechnic Institute and State University, Blacksburg, Virginia 24061

(Received 19 February 1996; accepted for publication 29 April 1996)

Polycrystalline $\text{Bi}_4\text{Ti}_3\text{O}_{12}$ thin films having layered perovskite structure were fabricated by metalorganic solution deposition technique on both Pt-coated Si and bare Si substrates at a temperature as low as 500 °C. The effects of post-deposition rapid thermal annealing on the structural and electrical properties were analyzed. The electrical measurements were conducted on metal-ferroelectric-metal capacitors. The typical measured small signal dielectric constant and dissipation factor at 100 kHz were 184 and 0.018 and the remanent polarization and the coercive field were 4.4 $\mu\text{C}/\text{cm}^2$ and 84 kV/cm, respectively. The films exhibited high resistivity in the range 10^8 – 10^{12} Ω cm for films annealed at temperatures of 500–700 °C for 10 s. The I – V characteristics were found to be Ohmic at low fields and space-charge-limited at high fields. A $V^{3/2}$ dependence of the current was observed in the space-charge region. This could be explained by assuming the mobility to be field dependent since in thin films the electric fields are invariably high even at low applied voltages. © 1996 American Institute of Physics. [S0021-8979(96)07615-3]

I. INTRODUCTION

Recently, there has been a surge in research activity on ferroelectric thin films for electronic devices such as pyroelectric infrared detectors, optical switches, actuators, displays, dynamic random access memories (DRAMs), and nonvolatile random access memories (NVRAMs).^{1–3} New synthesis and processing techniques are being developed for producing device quality films. Since $\text{Bi}_4\text{Ti}_3\text{O}_{12}$ was discovered by Aurivillius in 1949,⁴ layer structure ferroelectrics have been extensively studied. Among the many layer structure ferroelectric materials, bismuth related titanates show good ferroelectric properties. In particular, $\text{Bi}_4\text{Ti}_3\text{O}_{12}$ exhibits useful properties for optical memory, piezoelectric, and electro-optic devices.⁵ Bismuth titanate has high potential for device applications because of its relatively high dielectric constant, high Curie temperature, and high breakdown strength. The polarization vector in bismuth titanate lies in the a – c plane at an angle of about 4.5° to the a -axis.⁶ Hence there is a c -axis ($P_S=4$ $\mu\text{C}/\text{cm}^2$) and an a -axis ($P_S=50$ $\mu\text{C}/\text{cm}^2$) component of polarization. The low coercive field along the c -axis makes bismuth titanate an attractive gate electrode in a ferroelectric FET memory device of nondestructive readout (NDRO) mode.⁷ Ferroelectric thin films have attracted much attention for memory devices. However, there are still some problems that have to be solved prior to the realization of practical nonvolatile memory devices that utilize switching of ferroelectric polarization. Several problems concerning reliability, e.g., polarization fatigue, retention, imprint, and depolarization have served as major obstacles to the commercialization of high density nonvolatile memories.^{8,9} The ferroelectric thin films have several electrical problems such as dielectric and leakage current properties. The electrical conduction mechanism(s) in thin films are

not very well understood even though extensive studies have been done on the electrical and structural properties. The electrical properties of the films are dependent on the fabrication technique and the processing conditions. The relationship between the electrical properties and the crystal structure, such as lattice constant, film orientation, the average crystallite size, and nonuniform stress, must be elucidated. The present studies were aimed particularly at investigating the electrical behavior of $\text{Bi}_4\text{Ti}_3\text{O}_{12}$ thin films in relation to their structural characteristics. The effects of post-deposition rapid thermal processing on the structural and electrical properties of $\text{Bi}_4\text{Ti}_3\text{O}_{12}$ thin films were analyzed.

Several techniques such as rf sputtering,^{10,11} pulsed laser deposition,^{12,13} and electron cyclotron resonance plasma sputtering¹⁴ have been employed to deposit good quality $\text{Bi}_4\text{Ti}_3\text{O}_{12}$ thin films. In the present case, thin films of $\text{Bi}_4\text{Ti}_3\text{O}_{12}$ were fabricated using the metalorganic solution deposition (MOSD) technique.¹⁵ Recently, MOSD processing has been extensively used in thin film technology. Among the advantages of the MOSD techniques are low processing temperature, nonvacuum process, low equipment cost, precise composition control, and uniform deposition over a large substrate surface area. In the MOSD process, the as-grown films are amorphous in nature and post-deposition annealing is required to impart crystallinity. Post-deposition annealing of the films was carried out in a rapid thermal annealing (RTA) system. The RTA process has been widely used in the semiconductor industry for diverse applications,¹⁶ such as oxidation, doping, junction formation, and Ohmic contact formation. The great advantages of this method are a short annealing time and its relative process simplicity as compared with conventional furnace annealing. The objective of the short processing time is basically to reduce the temperature-time product such that the desired physical or chemical processes are completed while unwanted processes

^{a)}Electronic mail: pcjoshi@vt.edu

such as dopant diffusion, interface reactions, decomposition, or evaporation, etc., are suppressed or minimized. The short rise time to the desired annealing temperature minimizes the film-substrate interface reaction and results in dense microstructure. In this article, we report the structural and electrical properties of the rapid thermally processed $\text{Bi}_4\text{Ti}_3\text{O}_{12}$ thin films. The electrical properties reported include dielectric, ferroelectric, and current–voltage (I – V) characteristics.

II. EXPERIMENTAL PROCEDURE

Thin films of $\text{Bi}_4\text{Ti}_3\text{O}_{12}$ were fabricated by the MOSD technique using bismuth nitrate and titanium isopropoxide as precursors. Acetic acid and 2-methoxyethanol were selected as solvents. The precursor films were coated onto various substrates by spin coating using a photoresist spinner. The thickness of the films was controlled by adjusting the viscosity of the solution and the spin speed. Post-deposition annealing of the films was carried out in a 210T AG Associates rapid thermal annealing system at various temperatures in an oxygen atmosphere. The effects of annealing temperature on the structure and properties of the films were evaluated using a series of films deposited with a spinning speed of 4000 rpm for 20 s on bare Si and Pt-coated Si substrates. The structure of the films was analyzed by x-ray diffraction (XRD). The XRD patterns were recorded on a Scintag PAD-V diffractometer using $\text{Cu } K_\alpha$ radiation at 45 kV. The surface morphology of the films was analyzed by scanning electron microscopy (SEM). The thickness of the films was measured from SEM cross sections. The electrical measurements were conducted on films in a MFM capacitor configuration. Several gold dots of 0.6 mm diameter were evaporated through a mask over an area of $2 \text{ cm} \times 2 \text{ cm}$ on the films to form MFM capacitors. Capacitance and $\tan \delta$ values were measured in the 5 Hz–13 MHz frequency range with a HP 4192A impedance analyzer. Leakage current vs voltage characteristics were measured by means of a Keithley 617 electrometer/source.

III. RESULTS AND DISCUSSION

A. Structure

The pyrolyzed films (at $\sim 350^\circ\text{C}$) were found to be amorphous, and post-deposition annealing was required to develop crystallinity. Figure 1 shows the XRD patterns of the films, deposited on bare Si substrates and annealed by the RTA process, as a function of annealing temperature, while the annealing time was kept at 20 s. The results indicate that the duration of 20 s was enough to attain perovskite phase at 500°C . As the annealing temperature was increased, the peaks in the XRD pattern became sharper and the full width at half-maximum (FWHM) decreased indicating better crystallinity and an increase in grain size with increasing annealing temperature. The XRD patterns also revealed that films were polycrystalline in nature with no evidence of preferred orientation or secondary phases. The intensity and sharpness of the peaks was also found to increase with annealing time at a constant temperature. It was possible to induce the perovskite phase, with similar peak intensity and sharpness in the XRD pattern, at a lower annealing temperature by in-

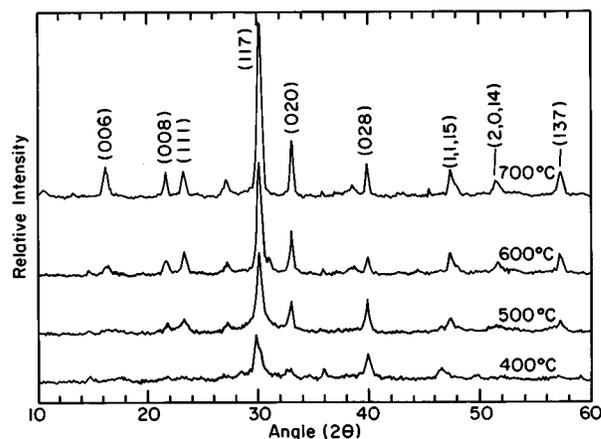


FIG. 1. X-ray diffraction patterns of $\text{Bi}_4\text{Ti}_3\text{O}_{12}$ films annealed by RTA process at various temperatures for 20 s.

creasing the annealing time, e.g., the intensity of the peaks in the XRD pattern for a film annealed at 500°C for 60 s was comparable to that of a film annealed at 700°C for 10 s.¹⁷ These results establish the significance of the RTA process to offer near-complete-phase formed films at relatively lower annealing temperatures.

The lattice constants a , b , and c were calculated using (020), (117), and (111) peaks in the XRD pattern, and were found to be 5.434, 5.430, and 32.74 \AA , respectively, for films annealed at 700°C for 10 s; suggesting that the films were crystallized in the orthorhombic phase. Similar values of lattice constants have been reported for polycrystalline $\text{Bi}_4\text{Ti}_3\text{O}_{12}$ thin films processed by other techniques. The lattice constant values were found to be slightly different from those of bulk $\text{Bi}_4\text{Ti}_3\text{O}_{12}$ ($a=5.510$, $b=5.448$, and $c=32.84 \text{ \AA}$). The slight difference between the thin film and bulk lattice constant values may be due to stress in the films since one surface of the film is clamped to the substrate. The stress may also arise due to thermal expansion mismatch between the film and substrate, due to structure and growth of the films. Table I lists the lattice constants of $\text{Bi}_4\text{Ti}_3\text{O}_{12}$ thin films annealed in the temperature range 500 – 700°C for a time of 10 s. It is clear from the table that as the annealing temperature was increased, both the a -axis and b -axis lattice constants increased while the c -axis lattice constant was un-

TABLE I. Lattice constants and grain size as a function of annealing temperature.

Annealing Temp/time $^\circ\text{C}/\text{s}$	Lattice constants (\AA)	Grain size (\AA) (XRD studies)	Grain size (\AA) (SEM studies)
500/10	$a=5.320$ $b=5.396$ $c=32.74$	328	600
600/10	$a=5.383$ $b=5.425$ $c=32.73$	454	1000
700/10	$a=5.434$ $b=5.430$ $c=32.74$	568	1670

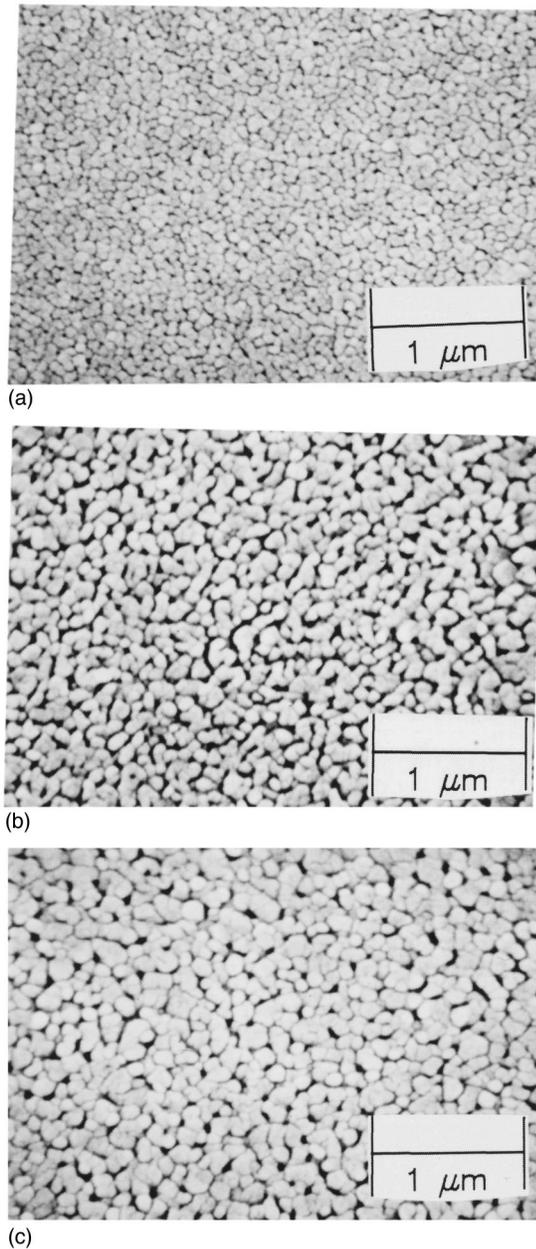


FIG. 2. SEM photographs of $\text{Bi}_4\text{Ti}_3\text{O}_{12}$ films annealed by RTA process at (a) 500 °C, (b) 600 °C, and (c) 700 °C.

changed. The values of a and b lattice constants approached the single crystal values with the increase in annealing temperature from 500 to 700 °C indicating the improvement in the ferroelectric orthorhombicity of the films. The changes in the lattice constants with increasing annealing temperature are related to the change of average crystallite size and/or decrease in the concentration of lattice imperfections due to decrease in the internal microstrain within the films.

B. SEM studies

The surface morphology of the as-pyrolyzed films was smooth. The films were crack-free and dense. The effects of the annealing temperature and film thickness on the morphology of the films were analyzed by SEM. Figure 2 shows the effects of post-deposition annealing on the grain size of

the films. The grain size increased with the increase in annealing temperature. Larger grain sizes are expected with increasing annealing temperature because of an increase in surface mobility, thus allowing the films to decrease its total energy by growing larger grains and decreasing its grain boundary area. The average grain size was in the range 0.06–0.167 μm for films annealed in the temperature range 500–700 °C for 10 s.

The average grain size G was also estimated from the half-width of the x-ray diffraction peaks using Scherrer's formula:¹⁸

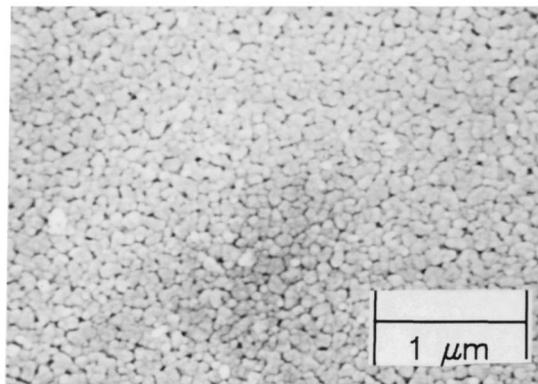
$$G = \frac{K\lambda}{\beta \cos \theta}, \quad (1)$$

where θ is the diffraction angle, λ is the average wavelength of the $\text{Cu } K\alpha$ radiation, K is the shape factor, and β is the line broadening. The constant K has a value of 0.9 when β is taken as half-maximum line breadth. Table I lists the grain size of the films annealed at different temperatures. The grain size was found to increase with the increase in annealing temperature. The grain sizes estimated by means of Scherrer's formula were much smaller than those estimated from SEM studies (Table I). The Scherrer formula assumes that all the crystallites are of the same size; but in an actual specimen, the size range and distribution affect β . Additionally, incoherent scattering from domains, distortions in the periodicity in the films, and micro-stresses contribute to line broadening and, hence, errors in the grain size estimation. So the x-ray line broadening yields relative crystallite sizes; absolute values are not readily obtainable by this method. Relative sizes are very useful in most applications, but if absolute sizes are necessary then other methods such as electron microscopy must be used to establish a basis for comparison.

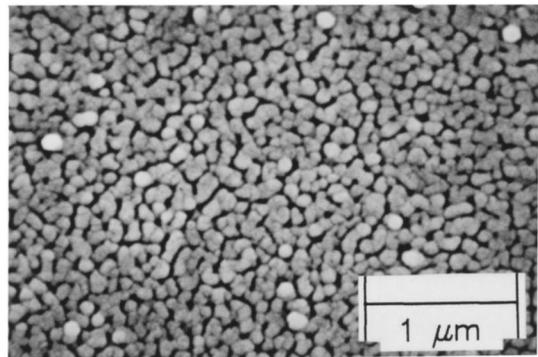
The grain size of the films was also found to be thickness dependent as shown in Fig. 3. The grain size increased with thickness up to about 0.4 μm , and beyond that, the increase was relatively small. The thickness dependence of the grain size explains the observed thickness dependence of the dielectric properties in the present films as discussed later. At smaller thicknesses, the grain size was found to be thickness dependent because the grain size was of the order of film thickness, indicating that the grain growth was not complete. As the thickness of the films was increased beyond 0.4 μm , the thickness dependence of the grain size was not appreciable. This may be due to completion of grain growth for larger film thicknesses. Similar thickness dependence of the grain size has also been reported for thin films of other dielectric materials.¹⁹ The density and grain formation through the thickness were also observed in the present $\text{Bi}_4\text{Ti}_3\text{O}_{12}$ films, in terms of cross-sectional SEM patterns. Figure 4 shows a typical cross-sectional SEM micrograph of a $\text{Bi}_4\text{Ti}_3\text{O}_{12}$ thin film. It may be seen from the figure that the films exhibited dense microstructure and uniform cross-sectional thickness.

C. Dielectric response

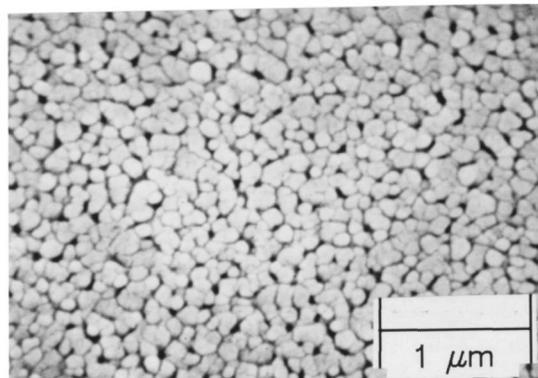
The dielectric properties of $\text{Bi}_4\text{Ti}_3\text{O}_{12}$ thin films was measured in terms of the dielectric constant ϵ_r and loss fac-



(a)



(b)



(c)

FIG. 3. SEM photographs of (a) 0.3 μm , (b) 0.5 μm , and (c) 0.8 μm thick $\text{Bi}_4\text{Ti}_3\text{O}_{12}$ films annealed by RTA process at 700 $^\circ\text{C}$ for 10 s.

tor $\tan \delta$. The applied electric field (~ 1.7 kV/cm) used for these measurements was considerably less than the coercive field of the material such that the ac field does not address the polarization state. This small signal applied to the films minimizes the domain wall contribution and allows the comparison of the thin film values with the bulk material. Figure 5 shows the low field dielectric constant and the dissipation factor as a function of frequency for a 0.5- μm -thick film annealed at 700 $^\circ\text{C}$ for 10 s. The small signal dielectric constant and the dissipation factor at a frequency of 100 kHz were 184 and 0.018, respectively. These values were found to be close to that of bulk $\text{Bi}_4\text{Ti}_3\text{O}_{12}$ and consistent with other reports.^{11,12} The permittivity showed no dispersion with frequency up to about 1 MHz, as shown in Fig. 5, indicating that the values were not masked by any surface layer effects or electrode barrier effects in this frequency

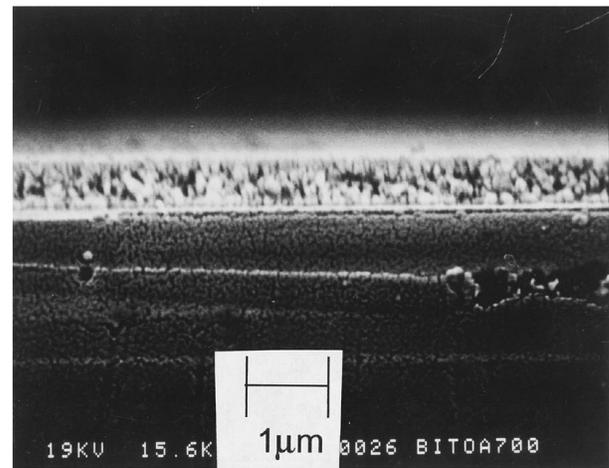


FIG. 4. Cross-sectional SEM photograph of $\text{Bi}_4\text{Ti}_3\text{O}_{12}$ film annealed by RTA process at 700 $^\circ\text{C}$ for 10 s.

region. The dielectric constant dropped abruptly to a small value as the frequency was increased above 1 MHz. At around the same frequency, the dissipation factor showed a very strong maximum. For any dielectric material, the intrinsic frequency dependence of the material or the effects due to electrodes or any internal interfacial barrier may induce such a resonance. Presence of an appreciable resistance, which may be arising from intrinsic or extrinsic sources, in series with the dielectric film can affect the dielectric response at high frequencies. Similar frequency dispersion behavior due to finite resistance of the external electrodes was also reported for other ferroelectric thin films.²⁰ In the present study, the resonance behavior was found to be extrinsic in nature as similar resonance was observed at around the same frequency for thin films of other dielectric materials having similar order of capacitance. At the frequencies of the order of a few MHz, the stray inductance L of the contacts and wires may induce an $L-C$ resonance at a resonant frequency f_r given by:

$$f_r = \frac{1}{2\pi\sqrt{LC}}, \quad (2)$$

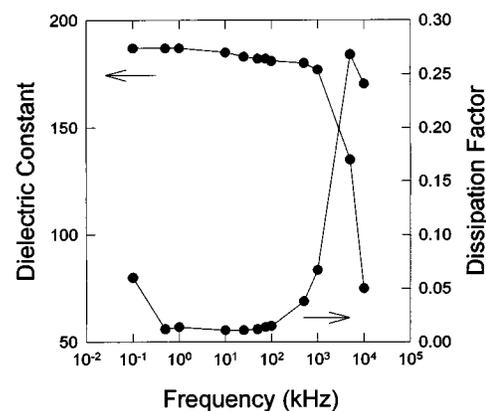


FIG. 5. Dielectric constant and dissipation factor as a function of frequency for $\text{Bi}_4\text{Ti}_3\text{O}_{12}$ film annealed at 700 $^\circ\text{C}$ for 10 s.

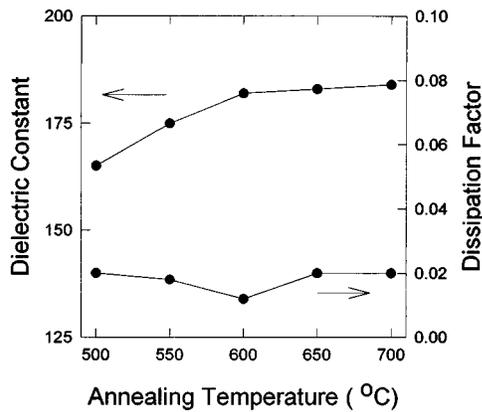


FIG. 6. Dielectric constant and dissipation factor as a function of annealing temperature for $\text{Bi}_4\text{Ti}_3\text{O}_{12}$ films annealed at various temperatures for 10 s.

where C is the capacitance of the sample under test. For thin films having capacitance of the order of 1 nF or so; a stray inductance of the order of a few micro-Henry can induce $L-C$ resonance in the mega-Hertz frequency range. As the resonance behavior was observed, in the present case around 2 MHz frequency, all the dielectric measurements were conducted at frequencies much lower than this resonance frequency. At these frequencies, the internal accuracy of the impedance analyzer was always better than 1%.

Figure 6 shows the dielectric constant and dissipation factor measured at 100 kHz as a function of annealing temperature. The dielectric constant increased with temperature up to about 600 °C and beyond that the increase was at a much lower rate. The dissipation factor was small and did not show any appreciable variation with temperature. The dielectric constant ranged from 167–184 for films annealed in the temperature range 500–700 °C for 10 s. In the present case, the XRD data and the SEM studies indicated an improvement in ferroelectric orthorhombicity and an increase in grain size with increasing annealing temperature. So the observed increase in dielectric constant with annealing temperature may be attributed to an increase in grain size and density of the films; which is consistent with other reports in the literature.²¹

Figure 7 shows the variation of the low field dielectric

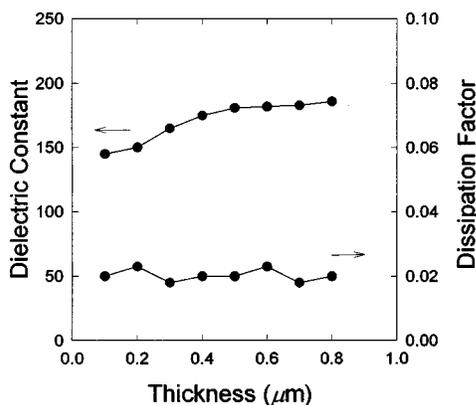


FIG. 7. Dielectric constant and dissipation factor as a function of thickness for $\text{Bi}_4\text{Ti}_3\text{O}_{12}$ films annealed at 700 °C for 10 s.

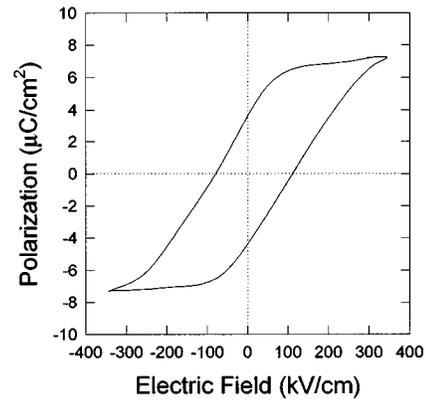


FIG. 8. Hysteresis loop measured at 500 Hz for a 0.5- μm -thick polycrystalline $\text{Bi}_4\text{Ti}_3\text{O}_{12}$ film on Pt-coated Si substrate.

constant and dissipation factor as a function of dielectric film thickness. The dielectric constant was found to increase with film thickness and attained a relatively constant value for film thicknesses greater than 0.4 μm . The dissipation factor did not show any appreciable variation with film thickness. A similar thickness dependence has been reported for thin films of other dielectric materials.²² The suggested explanations for such thickness dependence include stress in the films and the existence of barrier layer near one or both the electrodes. The stress resulting from the difference in the thermal expansion coefficient of the film and the substrate and that from the structure and growth of the films, which are generally found to have thickness dependence, may contribute to the thickness dependence of the dielectric constant in the present case. The thickness dependence of the grain size, as observed by the SEM studies in the present case, is also contributing to the thickness dependence of the dielectric constant. However, the possibility of surface layer effects at lower thicknesses may not be ignored.

D. Ferroelectric properties

Ferroelectric hysteresis measurements were conducted on 0.5- μm -thick $\text{Bi}_4\text{Ti}_3\text{O}_{12}$ films in a MFM configuration at room temperature. The dielectric loss was compensated in the measurements. Figure 8 shows a typical hysteresis loop of a film annealed at 700 °C for 10 s measured at a frequency of 500 Hz. The loops were measured by applying three cycles of an ac field of amplitude 350 kV/cm. The measured remanent polarization (P_r) was 4.4 $\mu\text{C}/\text{cm}^2$ and the coercive field (E_c) was 84 kV/cm. The measured polarization was slightly higher than the c -axis polarization of 4 $\mu\text{C}/\text{cm}^2$ observed in bulk $\text{Bi}_4\text{Ti}_3\text{O}_{12}$ single crystals⁶ and epitaxial films,²³ but it was small compared with the a -axis polarization of 50 $\mu\text{C}/\text{cm}^2$; however the value of the coercive field was found to be larger.

P_r and E_c were also measured as a function of annealing temperature. Figure 9 shows P_r and E_c as a function of annealing temperature for films annealed by the RTA process at temperatures of 500–700 °C for 10 s. The remanent polarization ranged from 3.3 to 4.4 $\mu\text{C}/\text{cm}^2$ and the coercive field was between 84 and 135 kV/cm under an applied electric field of 350 kV/cm. The trend may be found consistent

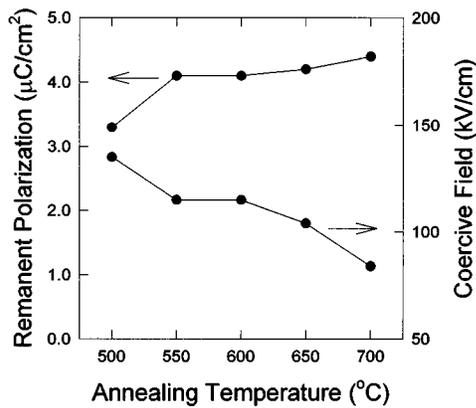


FIG. 9. Remanent polarization and coercive field as a function of annealing temperature for $\text{Bi}_4\text{Ti}_3\text{O}_{12}$ films annealed at temperatures of 500–700 °C for 10 s.

with the XRD and SEM data which indicate improvement in crystallinity with increasing annealing temperature. The decrease in E_c values with increasing annealing temperature could be attributed to the increase in grain size: the larger the grain size, the smaller the coercive field required to reverse the polarity of ferroelectric domains.

The effects of the frequency and amplitude of the oscillating field on the ferroelectric properties were studied. Figure 10 shows the dependence of the P_r and E_c on the frequency of the measuring signal. Both P_r and E_c values were found to decrease with increasing frequency. This is due, primarily, to the basic limitation on the speed at which the domains can switch. When a dipole switches from one state to another, there is a characteristic relaxation time associated with the change. If the period of the oscillating field is smaller than the relaxation time, then the dipole will not switch. Again, for a real collection of dipoles, this time may vary from dipole to dipole. At low frequencies, all of the dipoles will respond. At higher frequencies, dipoles with larger relaxation times will stop switching and the overall polarization decreases. Figure 11 shows the dependence of the P_r and E_c on the intensity of the oscillating field E . Both the remanent polarization and the coercive field values were found to increase with the increase in the amplitude of the

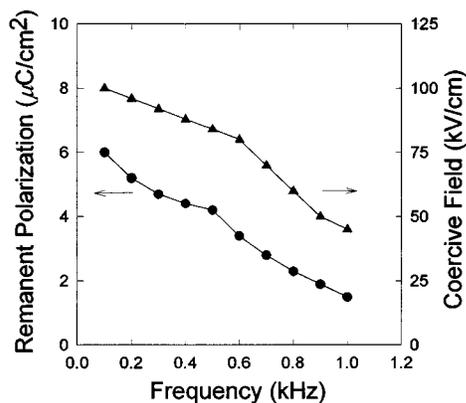


FIG. 10. The frequency response of the measured remanent polarization and coercive field of $\text{Bi}_4\text{Ti}_3\text{O}_{12}$ thin films in MFM configuration.

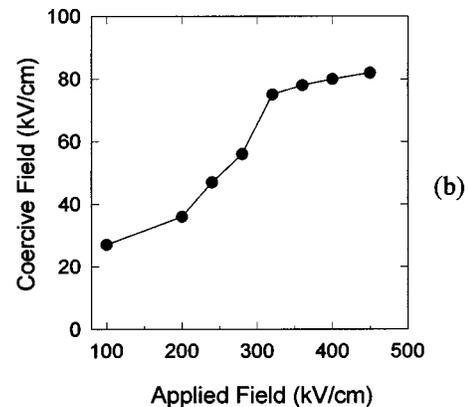
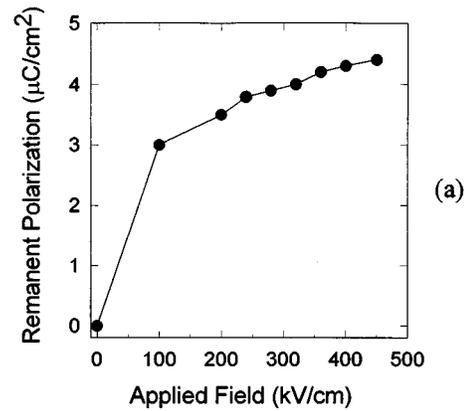


FIG. 11. Dependence of (a) remanent polarization, and (b) coercive field of $\text{Bi}_4\text{Ti}_3\text{O}_{12}$ thin films on the amplitude of the applied electric field.

applied field. The remanent polarization initially increased rapidly with applied field up to about 200 kV/cm. For larger fields, the P_r value increased rather linearly with the applied field indicating the complete switching of all the ferroelectric domains that could be switched. The increase in the coercive field value with the applied field may be attributed to increase in conductivity with increasing field.

E. I – V characteristics

The insulating properties of the films were found to be dependent on the post-deposition rapid thermal annealing treatment. As shown in Fig. 12, room temperature resistivity and leakage current density were greatly changed by the annealing temperature. The room temperature resistivity was found to increase with the increase in annealing temperature and was in the range of 10^8 – 10^{12} Ω cm up to 5 V corresponding to a field of 100 kV/cm across the capacitor for films annealed in the temperature range of 500–700 °C. The leakage current density decreased with the increase in annealing temperature. Typical leakage current density was lower than 10^{-8} A/cm² at an applied electric field of 100 kV/cm for films annealed at 700 °C for 10 s. Such reduction in leakage current density with increasing annealing temperature may be attributed to improved crystallinity and completeness of perovskite phase formation.

The mechanisms of transport of carriers through thin insulator films have been the subject of extensive theoretical and experimental investigations. These studies have been

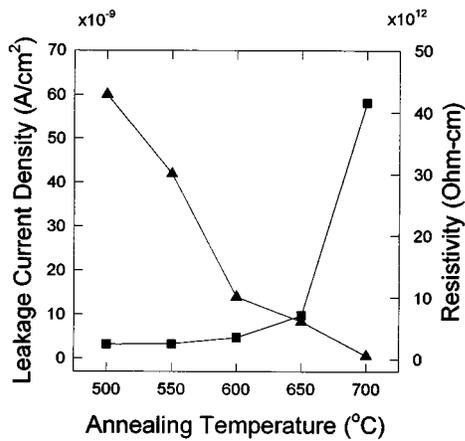


FIG. 12. Room temperature resistivity and leakage current density of $\text{Bi}_4\text{Ti}_3\text{O}_{12}$ films as a function of annealing temperature, measured at an applied electric field of 20 kV/cm.

stimulated by the attractive possibilities of development of a variety of miniaturized solid state devices. An understanding of the mechanism of nonlinear conductivity in thin insulators is pertinent to the development of thin film devices for microelectronics. The steady state field dependent dc conductivity was examined through the measurement of the $I-V$ characteristics in MFM capacitors. Several electrical processes allow electrical charges to move in insulators, leading to sizable current densities. For thin insulating films of the order of 1 μm , if an appreciable voltage can be sustained (of the order of few volts), the field strength is of the order of 10^5 V/cm and greater. The low field electrical properties are usually Ohmic in nature, that is, current I is linear with voltage V . At high fields, these films exhibit nonlinear $I-V$ relationship. Their non-Ohmic behavior can be expressed by the empirical power law $I = KV^\alpha$. Generally, the high field electrical characteristics can not be adequately described by a single conduction process; usually the different field strength ranges manifest different electrical phenomena.

Figure 13 shows the $I-V$ characteristics as a function of thickness for films annealed at 700 °C for 10 s. The thickness dependence of the $I-V$ characteristics indicated bulk limited conduction.²⁴ There was no change in the conductivity with

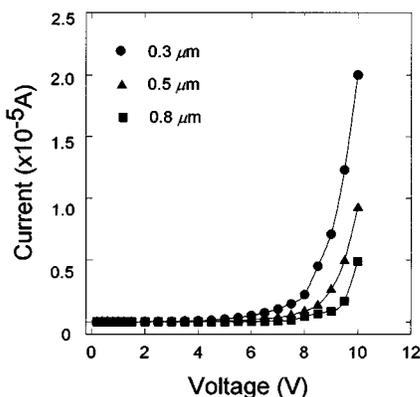


FIG. 13. $I-V$ characteristics of $\text{Bi}_4\text{Ti}_3\text{O}_{12}$ thin films exhibiting thickness dependence.

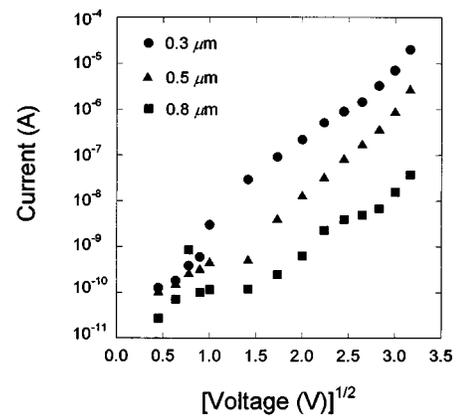


FIG. 14. $I-V$ characteristics plotted as $\log(I)$ vs $V^{1/2}$. The nonlinearity indicated the absence of the Poole-Frenkel effect.

the change in the polarity of the applied voltage, which also indicated the conduction process to be bulk limited and not electrode limited. These films exhibited high resistivities in the range of 10^8 – 10^{12} Ω cm, at an applied electric field of 100 kV/cm, for 100–800 nm thick films. In this range of resistivities, the possible dominant conduction mechanism may be (a) tunneling, (b) Poole-Frenkel effect, and/or (c) space-charge-limited-current (SCLC) conduction. As the thickness of the films was well above 0.05 μm , the tunneling process was ruled out. If the non-Ohmic conduction is due to Poole-Frenkel flow, then we should get a straight line in $\log(I)$ against $V^{1/2}$ plots, which was not found in the present case, as can be seen from Fig. 14. So the dominant bulk limited conduction at high fields was expected to be space-charge-limited current conduction. Figure 15 shows the $\log(I)$ versus $\log(V)$ plot for a 0.8- μm -thick film measured at room temperature. The general features of $I-V$ characteristics, namely a linear regime followed by a superlinear one, gave evidence to current injection which for a highly resistive material is space-charge-limited. At very low voltages, the slope of the $\log(I)$ vs $\log(V)$ plot was approximately unity which corresponded to the Ohmic law region as expected from the theory of SCLC conduction. This Ohmic region in the films extended to very low voltages of up to

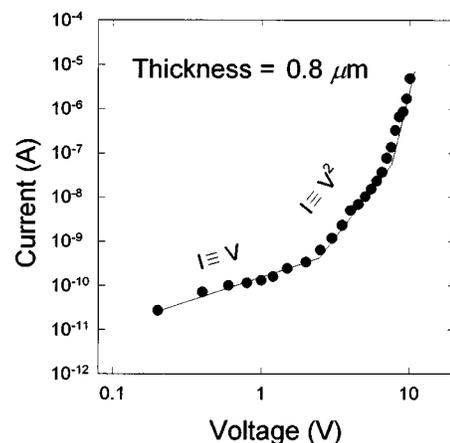


FIG. 15. Typical $\log(I)$ vs $\log(V)$ curve for a 0.8- μm -thick $\text{Bi}_4\text{Ti}_3\text{O}_{12}$ film. Solid line represents the best fit to the data.

about 1 V. According to SCLC theory, this Ohmic mode occurs in insulating film as long as the film is quasi-neutral, i.e., as long as the bulk generated current in the film exceeds the current due to injected free carriers from the electrode. The $I-V$ dependence in the Ohmic region is given by:²⁵

$$I = \frac{qn\mu AV}{d}, \quad (3)$$

where q is the electronic charge, d is the film thickness, n is the concentration of charge carriers, μ is the mobility, and A is the area of the electrodes. An enhanced voltage dependence occurred, as shown in Fig. 15, for voltages of more than 1 V. According to the SCLC theory, as the applied voltage is increased, a strong injection of the charge carriers in the bulk of the film takes place. For stronger injection, the insulator traps fill up and a space charge appears. The space-charge effects are observed when the injected free carrier density exceeds the volume generated free carrier density. The slope of this nonlinear regime, calculated from the $\log(I)$ vs $\log(V)$ plot, was about 1.5 indicating onset of the bulk limited space-charge conduction. The SCLC in a trap free insulator is given by:²⁵

$$I = \frac{9A\epsilon_r\epsilon_0\mu V^2}{8d^3}, \quad (4)$$

where ϵ_r is the dielectric constant of the film and ϵ_0 is the permittivity of free space. In the presence of single shallow trapping level, Eq. (4) is replaced by:²⁵

$$I = \frac{9\theta A\epsilon_r\epsilon_0\mu V^2}{8d^3}, \quad (5)$$

where θ is the ratio of the free electron density and the density of the filled trapping sites. Eq. (5) also holds well for an exponential distribution of traps. The calculated slope of 1.5 in the high field regime was slightly lower than the slope of 2 as expected from Eq. (5). In thin films, the voltages are such that the electric field invariably crosses the low field limit, i.e., at 10^3 V/cm. Also in the present study, the field is high. The observed discrepancy in the slope of the $I-V$ curves in the high field regime can be explained by a simple model of field dependent mobility. The field dependence of mobility has been analyzed for a number of different materials while studying the SCLC through insulators. At high fields, the mobility μ —assuming that the drift velocity varies as square root of the applied field—may approximately be written as:²⁶

$$\mu = \mu_0 E_0^{1/2} E^{-1/2}, \quad (6)$$

where μ_0 is the low field; field independent mobility, E is the applied electric field, and E_0 is the critical field beyond which the field dependence of the mobility is dominant. The Poisson equation, for a single shallow trapping level, can be written as:

$$\frac{dE}{dx} = \frac{qn}{\theta\epsilon_r\epsilon_0}. \quad (7)$$

By solving the Poisson equation, using Eqs. (3) and (6), we get

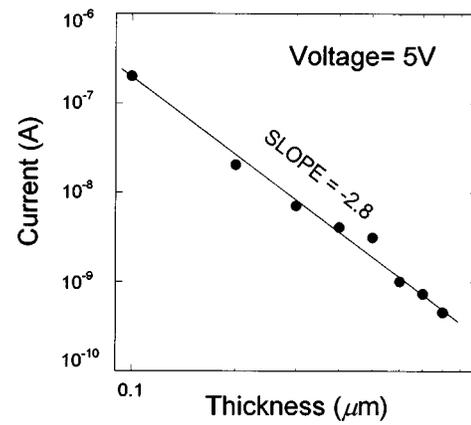


FIG. 16. $\log(d)$ plotted against $\log(I)$ at 5 V corresponding to space-charge region.

$$J = K_1 \frac{V^{3/2}}{d^{5/2}}, \quad (8)$$

where

$$K_1 = \frac{2}{3} \left(\frac{5}{3} \right)^{3/2} \theta A \epsilon_r \epsilon_0 \mu_0 E_0^{1/2}.$$

So a slope of 1.5 is expected in the high field region when the mobility is assumed to be field dependent. As the applied electric fields are invariably high in thin films, so a field dependence of mobility must always be considered. The effects of $\text{Bi}_4\text{Ti}_3\text{O}_{12}$ film thickness were also investigated in the range where $I \propto V^{3/2}$, by plotting $\log(I)$ vs $\log(d)$ at 5 V corresponding to space-charge region. The slope of the straight line, as shown in Fig. 16, drawn through the experimental points was about -2.75 . This value is slightly lower than the value expected from Eq. (8) but slightly higher than the value of -3 expected from Eq. (5). The field dependence of mobility is rather complicated in form and the thickness dependence is uncertain.²⁷ The electron drift in the conduction band is marked by frequent collisions with the thermal vibrations, the impurities, and the structural defects in the material. The various powers of V and d have been found to satisfy the observed SCLC conduction in the insulating films of a number of different materials. This space-charge region should be followed by a second square law region corresponding to trap limited space-charge conduction due to very strong injection of the charge carriers at higher applied voltages. If sufficient charge is injected into the insulator, all traps will become filled. Further injected charge then exists as free charge in the conduction band and contributes to the current. The current expression is identical to Eq. (8) when using $\theta=1$. In the present case, no apparent trap filled limit was observed even up to an applied voltage of 15 V.

IV. CONCLUSIONS

Polycrystalline $\text{Bi}_4\text{Ti}_3\text{O}_{12}$ thin films exhibiting good structural, dielectric, and ferroelectric properties were successfully produced on both Pt-coated Si and bare Si substrates by combination of the MOSD technique and rapid thermal annealing. The surface morphology of the films was

smooth with no cracks and defects while the grain size was found to increase with increasing in the annealing temperature. The grain size increased with film thickness up to about $0.4\ \mu\text{m}$ and beyond that the increase was relatively small. The thickness dependence of the grain size was significant in the region where the grain size was of the order of film thickness. For a film annealed at $700\ ^\circ\text{C}$ for 10 s, the small signal dielectric constant and dissipation factor at 100 kHz were 184 and 0.018, respectively. The dielectric properties were found to be thickness and annealing temperature dependent due to thickness and annealing temperature dependence of the grain size as verified from SEM observations. The measured remanent polarization and the coercive field were $4.4\ \mu\text{C}/\text{cm}^2$ and $84\ \text{kV}/\text{cm}$, respectively, for a film annealed at $700\ ^\circ\text{C}$ for 10 s. The ferroelectric properties were also found to depend on the post-deposition rapid thermal annealing treatment, and the frequency and amplitude of the applied electric field. The remanent polarization ranged from 3.3 to $4.4\ \mu\text{C}/\text{cm}^2$ and the coercive field was between 84 and $135\ \text{kV}/\text{cm}$ under an applied electric field of $350\ \text{kV}/\text{cm}$ for films annealed in the temperature range 500 – $700\ ^\circ\text{C}$. Room temperature resistivity and leakage current were greatly influenced by the annealing temperature. The room temperature resistivity was in the range 10^8 – $10^{12}\ \Omega\ \text{cm}$ at an applied electric field of $100\ \text{kV}/\text{cm}$ for films annealed in the temperature range 500 – $700\ ^\circ\text{C}$. The dominant electrical conduction mechanism was found to be SCLC conduction. The I – V characteristics showed Ohmic conductivity in the lower voltage range and space-charge-limited conductivity in the higher voltage range. In the space-charge-limited region, a $V^{3/2}$ dependence of the current was found. This was explained by a simple model of field dependent mobility. The present studies re-emphasize the need to correlate the electrical characteristics of thin films with their structural properties and the measurement conditions.

- ¹C. A. Paz de Araujo, L. D. McMillan, B. M. Melnick, J. D. Cuchiaro, and J. F. Scott, *Ferroelectrics* **104**, 241 (1990).
- ²G. H. Haertling, *J. Vac. Sci. Technol.* **9**, 414 (1990).
- ³M. H. Francombe and S. V. Krishnaswamy, *J. Vac. Sci. Technol. A* **8**, 1382 (1990).
- ⁴B. Aurivillius, *Ariv Kemi* **1**, 463 (1949).
- ⁵S. Y. Wu, W. J. Takei, and M. H. Francombe, *Ferroelectrics* **10**, 209 (1976).
- ⁶S. E. Cummins and L. E. Cross, *J. Appl. Phys.* **39**, 2268 (1968).
- ⁷H. Buhay, S. Sinharoy, W. H. Kasner, M. H. Francombe, D. R. Lampe, and E. Stepke, *Appl. Phys. Lett.* **58**, 1470 (1991).
- ⁸S. B. Desu, *Phys. Status Solidi (a)* **151**, 467 (1995).
- ⁹J. J. Lee, C. L. Thio, and S. B. Desu, *Phys. Status Solidi (a)* **151**, 171 (1995).
- ¹⁰T. S. Kalkur, J. Kulkarni, Y. C. Lu, M. Rowe, W. Han, and L. Kammerdiner, *Ferroelectrics* **116**, 135 (1991).
- ¹¹M. Yamaguchi, T. Nagatomo, and O. Omoto, *Jpn. J. Appl. Phys.* **34**, 5116 (1995).
- ¹²N. Maffei and S. B. Krupanidhi, *Appl. Phys. Lett.* **60**, 781 (1992).
- ¹³W. Wu, K. Fumoto, Y. Oishi, M. Okuyama, and Y. Hamakawa, *Jpn. J. Appl. Phys.* **34**, 5141 (1995).
- ¹⁴H. Masumoto, T. Goto, Y. Masuda, A. Baba, and T. Hirai, *Appl. Phys. Lett.* **58**, 243 (1991).
- ¹⁵P. C. Joshi, A. Mansingh, M. N. Kamalasanan, and S. Chandra, *Appl. Phys. Lett.* **59**, 2389 (1991).
- ¹⁶R. Singh, *J. Appl. Phys.* **63**, R59 (1988).
- ¹⁷P. C. Joshi and S. B. Krupanidhi, *J. Appl. Phys.* **72**, 5827 (1992).
- ¹⁸P. Scherrer, *Gottinger Nachr.* **2**, 98 (1918).
- ¹⁹J. Park and W. Grannemann, *Ferroelectrics* **10**, 217 (1976).
- ²⁰M. Sayer, A. Mansingh, A. K. Arora, and A. Lo, *Integrated Ferroelectrics* **1**, 129 (1992).
- ²¹K. Okazaki and K. Nagata, *J. Am. Ceram. Soc.* **56**, 82 (1973).
- ²²C. Feldman, *J. Appl. Phys.* **65**, 872 (1989).
- ²³W. J. Takei, N. P. Formigoni, and M. H. Francombe, *J. Vac. Sci. Technol.* **7**, 442 (1970).
- ²⁴M. Stuart, *Phys. Status Solidi* **23**, 595 (1967).
- ²⁵J. G. Simmons, in *Handbook of Thin Film Technology*, edited by L. I. Maissel and R. Glang (McGraw-Hill, New York, 1970), pp. 14–35.
- ²⁶M. A. Lampert and P. Mark, *Current Injection in Solids* (Academic, New York, 1970).
- ²⁷K. L. Chopra, *Thin Film Phenomena* (McGraw-Hill, New York, 1969).